THE JOURNAL OF PHYSICAL CHEMISTRY C

Article

Cite This: J. Phys. Chem. C 2019, 123, 19844−19850

pubs.acs.org/JPCC

Direct and Indirect Recombination and Thermal Kinetics of Excitons in Colloidal All-Inorganic Lead Halide Perovskite Nanocrystals

Huafeng Shi,[†,‡] Xiaoli Zhang,[†] Xiaowei Sun,[†] Rui Chen,*[,†] and Xinhai Zhang*[,†]

[†]Department of Electrical and Electronic Engineering, Southern University of Science and Technology, Shenzhen 518055, China

[‡]Harbin Institute of Technology, Harbin 150001, China

Supporting Information

ABSTRACT: In recent years, the colloidal all-inorganic lead halide perovskite nanocrystal has become one of the most notable optoelectronic materials. The kinetics of excitons directly influence the device performance, but it is very complicated and still unclear. Here, we have presented the investigation of thermal kinetics of excitons in colloidal all-inorganic lead halide perovskite nanocrystals. As temperature increases from 4 K to room temperature, the photoluminescence (PL) intensity follows the Arrhenius equation with interruption at 130−150 K, while the average PL lifetime follows the double-Boltzmann function fitting, discontinuing at the same temperature. These experimental results could be explained by direct and indirect recombination of excitons. The excitons directly recombine with a short lifetime of about 300 ps. Indirect recombination is completed by the photo-excited electrons (holes) along the path of trapping, detrapping, and then recombination with holes (electrons). The excitons mainly undergo indirect recombination at low temperature and balance at the temperature of 130−150 K because of thermal activation, while direct recombination happens at high temperature. Our experimental results provide insight into the recombination mechanism of excitons in colloidal all-inorganic lead halide perovskite nanocrystals, which will be helpful to unravel their potential for high-performance optoelectronic devices.

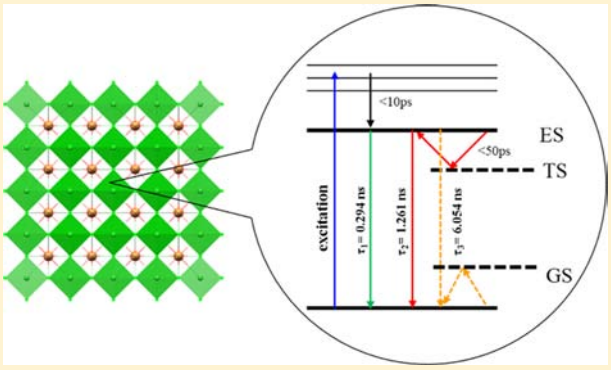

INTRODUCTION

Lead halide perovskites have been recognized as a promising functional material for optoelectronic device applications, including high-efficiency photovoltaic cells,[1] light-emitting diodes,[2,3] terahertz source,[4,5] photo detectors,[6] and other optoelectronic functional devices.[7,8] All-inorganic lead halide perovskite shows high stability compared to those organic ones, which have attracted intensive research attention.[9,10] Bulk crystal of all-inorganic lead halide perovskite showed poor photoluminescence (PL) because of the ionic characteristic which leads to the dissociation of excitons.[11] However, with size reduction to the nanoscale, extraordinary properties have been produced.[3,12] Colloidal all-inorganic lead halide perovskite nanocrystals present wide and tunable absorption ability, narrow emission, strong luminescence, and excellent PL quantum yield even up to nearly 100%.[13] Therefore, colloidal all-inorganic lead halide perovskite nanocrystals have been considered as a promising optoelectronic material.

The kinetics of carriers during the photo-excitation process in colloidal all-inorganic lead halide perovskite nanocrystals is very complicated, which directly influences the device performance. Random formation of charged carriers and the associated nonradiative Auger recombination result in emission blinking.[14,15] The decay of charged carriers in perovskite is caused by much faster Auger recombination than common quantum dots and seems to deviate from "universal volume scaling".[16,17] Dark states for carriers may suppress PL emission and could mix with bright states under thermal activation.[18−20] Self-trapped carriers in perovskite that could produce warm white light break the band gap limitation.[21,22] Different diffusion of electrons and holes could generate terahertz emission.[4,5] Alkali cation (Cs) could lead to a more homogeneous spacing between various lattice planes for increasing carrier lifetime and charge recombination.[23] The band bending of grain boundaries in mixed phases could improve photocurrent performance of all-inorganic lead halide perovskite.[24] To fully realize the potential of perovskites, it is imperative to obtain a deeper understanding of the underlying photophysics of all-inorganic lead halide perovskite nanocrystals.

During the photon excitation of the perovskite $CsPbBr_3$ nanocrystal, photo-excited carriers may exist as the exciton (bound electron−hole pair), biexciton (double bound electron−hole pair), and trion (charged exciton, electron−hole pair bounding one more electron). The direct recombination of the exciton could be fitted by single-

Received: May 13, 2019
Revised: July 16, 2019
Published: July 24, 2019

DOI: 10.1021/acs.jpcc.9b04532
J. Phys. Chem. C 2019, 123, 19844−19850

exponential decay perfectly with a time constant around 300 ps for the $CsPbBr_3$ nanocrystal.[14−16,25,26] Biexcitons have much shorter decay time because of faster Auger recombination.[27−33] For the solution-synthesis method, surface organic ligands are necessary to monodisperse the perovskite nanocrystal, which could also lead to defect states in the perovskite nanocrystal.[34,35] The dark state has also been observed in the perovskite nanocrystal at cryogenic temperature, similar to the CdSe nanocrystal.[3] The double exponential function could be used to describe these PL decay including the biexciton and defect/dark state. Trions need higher excitation power and always come along with the exciton and biexciton in the perovskite $CsPbBr_3$ nanocrystal. PL decay could be fitted by the tri-exponential function.[31,36] PL dynamics in the perovskite $CsPbBr_3$ nanocrystal strongly depends on temperature, and therefore, tri-exponential fitting is often used to analyze these experimental data.[13] It is necessary to mention that the temperature-dependent PL is obviously different from the process including excitons, biexcitons, and trions. The thermal kinetics need more information to determine physical processes when temperature changes. Also, the mechanism responsible for long PL lifetimes observed in many lead halide perovskites is still under debate.[37]

Here, we have presented the investigation of the exciton dynamics in the colloidal all-inorganic lead halide perovskite nanocrystal. At room temperature (293 K), steady-state PL demonstrates a linear relationship with excitation power while maintaining the same shape. As temperature increases from 4 K to room temperature, the integrated PL intensity follows the Arrhenius equation with an interruption at 130−150 K. The temperature-dependent time-resolved PL (TRPL) data show that the average PL lifetime follows the double-Boltzmann function, which also shows a turning point at the same temperature. The experimental data could be fitted by using the tri-exponential function. The exciton is directly recombined with a short lifetime of about 300 ps. The indirect recombination is due to the photo-excited electrons (holes) along the path of trapping, detrapping, and recombination with holes (electrons), corresponding to the intermediate (long) lifetime. The direct and indirect recombination has a balance at the temperature of 130−150 K. Our experimental results provide insight into the direct and indirect recombination mechanism for excitons in the colloidal all-inorganic lead halide perovskite nanocrystal, which is helpful to unravel their potential for high-performance optoelectronic devices.

METHODS

The colloidal all-inorganic lead halide perovskite nanocrystal samples were synthesized using the hot-injection method,[9] and a detailed description of the synthesis procedures can be seen in the Supporting Information. The steady-state PL spectra were measured by using a spectrometer (SP2300) with a CCD detector (PIX400BRX) under excitation by He−Cd gas laser with a wavelength of 325 nm. The sample was mounted with silver paint on the cold finger of a Janis closed-cycle cryostat, providing a varying temperature range from 4 K to room temperature (293 K). The lifetime of samples were measured by a time-correlated single photo counting system under excitation of 375 nm pulse laser (~40 ps).

RESULTS AND DISCUSSION

The characteristic of the perovskite nanocrystal is shown in Figure 1. The X-ray diffraction (XRD) results of perovskite

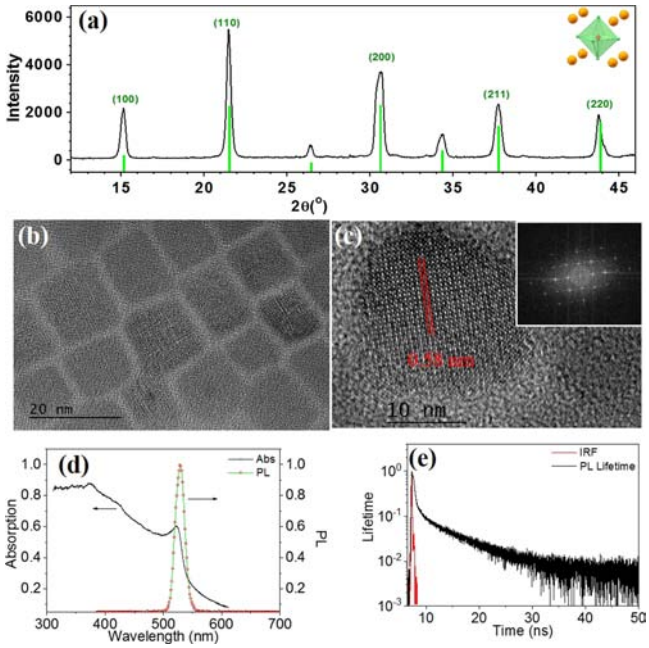

Figure 1. Characteristics of the colloidal all-inorganic lead halide perovskite $CsPbBr_3$ nanocrystal. (a) XRD results of the perovskite $CsPbBr_3$ nanocrystal and inset common cubic phase. (b) TEM results of the perovskite $CsPbBr_3$ nanocrystal. (c) HRTEM results and lattice diffraction pattern of the perovskite $CsPbBr_3$ nanocrystal. (d) Absorption and PL spectra of the perovskite $CsPbBr_3$ nanocrystal at room temperature. (e) TRPL of the perovskite $CsPbBr_3$ nanocrystal at room temperature.

samples are shown in Figure 1a. There are five strong peaks located at 15.19°, 21.55°, 30.64°, 37.75°, and 43.89°, which can be attributed to the (100), (110), (200), (211), and (220) faces of the cubic phase of $CsPbBr_3$ (ICSD no. 00-054-0752), respectively. The inset of Figure 1a shows the common cubic phase of the perovskite $CsPbBr_3$ nanocrystal. The transmission electron microscope (TEM) results indicate that the perovskite $CsPbBr_3$ nanocrystal is monodispersed with a size of about 15 × 15 nm, as shown in Figure 1b. Surface ligands adsorbed on the nanocrystal's surface separate the neighboring perovskite $CsPbBr_3$ nanocrystals. The electron beam of TEM could reshape the morphology of the perovskite nanocrystal. As shown in the high-resolution TEM (HRTEM) of single perovskite nanocrystal, four direct corners of the nanocrystal cube shape disappear and the center of the nanocrystal cube can be seen more clearly as in Figure 1c. The distance of the nearest neighboring atoms in both the vertical and horizontal directions are about 0.58 nm, which agrees well with the (100) face value of the cubic phase of $CsPbBr_3$. Figure 1d shows the absorption and the PL spectra of the perovskite $CsPbBr_3$ nanocrystal measured at room temperature. The absorption edge is identified by the sharp band edge and excitonic feature at about 522 nm.[38] The PL peak position is around 524 nm with a width of about 20 nm, which slightly red-shifted from the excitonic peak position. This red-shift phenomenon, also known as Stokes shift, is commonly observed in perovskite, which may be ascribed to the spectral diffusion-exciton

DOI: 10.1021/acs.jpcc.9b04532
J. Phys. Chem. C 2019, 123, 19844−19850

relaxation process.[39,40] The TRPL curves are necessary to analyze the physical process of the emission in the perovskite $CsPbBr_3$ nanocrystal, illustrating in Figure 1e. The average PL lifetime of the perovskite $CsPbBr_3$ nanocrystal is about 2 ns. Note that it is orders of magnitude faster than other optoelectronic materials with a typical decay time (larger than 100 ns), such as CdSe, ZnO, and Au nano-particles.[41−44] This makes the perovskite nanocrystal suitable for application in light-emitting diodes, light display, lasers, photodetectors, and other optoelectronic devices.

Excitation Power-Dependent PL Measurement at Room Temperature. Under continuous wave (CW) laser (325 nm) excitation, we measured the steady-state PL with various excitation powers at room temperature, as shown in Figure 2. To determine the integrated PL intensity I_{PL}, the

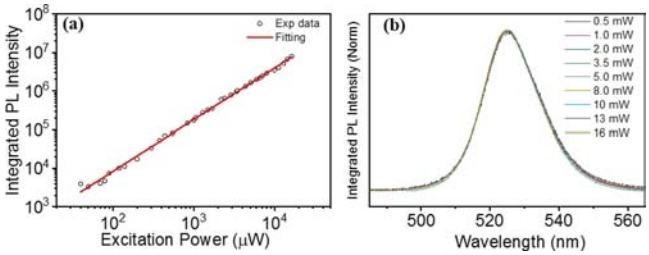

Figure 2. PL with increasing excitation power. (a) Integrated PL intensity linearly increasing with excitation power. (b) PL line-shape invariant with excitation power.

average excitation power was controlled from 4 μW to 18 mW. As shown in Figure 2a, I_{PL} shows a linear relationship with the excitation laser power I_{ex}, and the slope is about 1.34, which is under full thermal equilibrium conditions. There is no saturation effect or rapid increase observed with increasing excitation power. It means that the PL is mainly due to the spontaneous radiation rather than amplified spontaneous emission or other optical nonlinear phenomenon.[36,45] For the normalized PL spectra, no obvious peak shift or broadening can be observed, as shown in Figure 2b.

Temperature-Dependent PL Measurement. Figure 3 shows the temperature-dependent PL of the perovskite $CsPbBr_3$ nanocrystal from 4 K to room temperature. The PL spectra were obtained under an excitation power of 20 μW by a 325 nm CW laser, as shown in Figure S3. Lower excitation power is necessary to discuss the intrinsic emission processes, avoiding the heating effect,[46−49] lattice expansion,[50] and structural transition[51] induced by intensive laser excitation. As the temperature increases from 4 K to room temperature, the peak position has a blue-shift (530−524 nm) and the peak width broadening (6 to nearly 20 nm), as shown in Figure 3a. The band gap theory could be used to explain the temperature-dependent PL peak position.[52] As the temperature increases, the band gap narrowing about 27 meV results in the PL peak position blue-shift from 530 to 524 nm, as shown in Figure 3b. The broaden PL peak width can be attributed to the phonon-assisted broadening effect.

As the temperature increases, the integrated PL intensity shows a monotonic decrease which interrupts at 130−150 K, where the integrated PL intensity slightly increases and then continues to decrease, as shown in Figure 3c. As the temperature increases, more excitation energy transfers to the lattice and other electrons, which results in the decreased integrated PL intensity. The temperature-dependent PL data

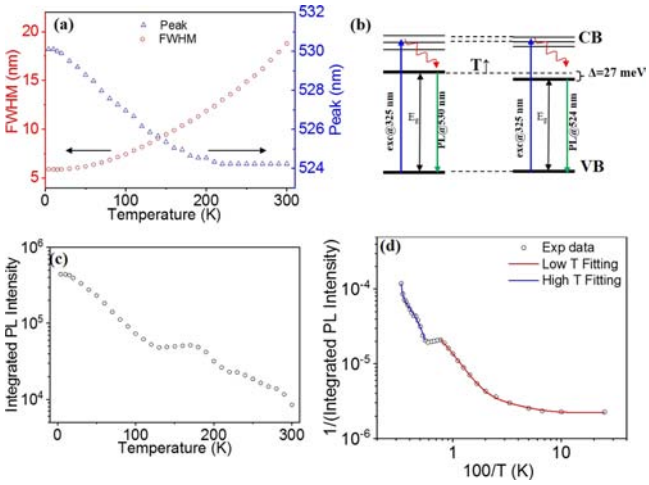

Figure 3. Temperature-dependent PL spectra of the perovskite $CsPbBr_3$ nanocrystal. (a) Integrated PL intensity with temperature. (b) Peak position and width of PL with temperature. (c) Reciprocal integrated PL intensity with reciprocal temperature (amplified a hundred times). (d) Diagram describing the temperature-dependent PL.

could be described by the Arrhenius equation as given below[38,45]

$$\frac{I_0}{I_{(T)}} = 1 + A_1\, e^{-E_1/kT} + A_2\, e^{-E_2/kT} \quad (1)$$

I_0 is the integrated PL intensity at 0 K. $I_{(T)}$ is the integrated PL intensity at temperature T. A_1 (A_2) relates to the density of recombination centers. E_1 (E_2) is the activation energy of recombination center.

The temperature-dependent PL could be fitted by the Arrhenius equation, respectively, in two ranges of low temperature (red solid line) and high temperature (blue solid line), which is separated by the interruption (130−150 K), as shown in Figure 3d. As indicated from the PL process, photo-excited carriers may exist as excitons, biexcitons, and trions; and the carrier recombination may have direct or indirect recombination. As the temperature increases, population of biexcitons and trions raise because of the photon-phonon coupling effect,[53] which may result in slight emission increase and then continues to decrease. However, the biexciton and trion are hard to exist in perovskite at very low excitation power. Moreover, there are no obvious information in the PL peak position and width, which could evidence the existence of the biexciton and trion. Thus, carrier's recombination may play a major role. To further analyze the mechanism, TRPL characterizations are necessary, as the following results in Figure 4.

Temperature-Dependent Evolution of Carriers' Dynamics. At room temperature, the PL decay contains two lifetimes with different time scales, a fast decay and a slow decay, as shown in Figure 4a. To further analyze the physical process, TRPL measurement was performed from 4 K to room temperature. The temperature-dependent TRPL of the perovskite $CsPbBr_3$ nanocrystal is illustrated in Figure 4b. These TRPL results could be fitted with a tri-exponential function convoluted with the instrument response function (IRF) to obtain the accurate average PL lifetime[13]

DOI: 10.1021/acs.jpcc.9b04532
J. Phys. Chem. C 2019, 123, 19844−19850

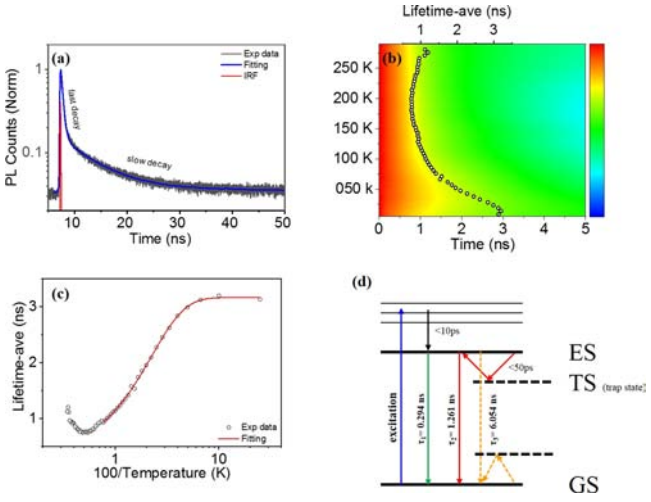

Figure 4. Temperature-dependent PL lifetime of the perovskite $CsPbBr_3$ nanocrystal. (a) Fast and slow decay of PL lifetime. (b) Color mapping of temperature-dependent PL lifetime and the average value. (c) Double-Boltzmann function fitting lifetime at 4 K and room temperature. (d) Diagram of the exciton direct and indirect recombination.

$$I_{\mathrm{conv}}(t) = \int_0^t \mathrm{IRF}(t^*) \sum_{i=1}^{3} A_i \, \mathrm{e}^{-t-t^*/\tau_i} \, \mathrm{d}t^* \tag{2}$$

$$\tau_{\mathrm{av}} = \sum_{i=1}^{3} A_i \tau_i^2 / \sum_{i=1}^{3} A_i \tau_i \tag{3}$$

$I_{\mathrm{conv}}(t)$ is the convolved model decay that is to be compared to the measured decay. $A_i \, \mathrm{e}^{-t-t*/\tau_i}$ is the model decay law. τ_{av} is the average PL lifetimes. IRF(t^*) is the normalized measured IRF.

All these TRPL curves could be globally fitted smoothly with a short time (τ_1 = 0.294 ns), an intermediate time (τ_2 = 1.261 ns), and a long time (τ_3 = 6.054 ns) with different amplitudes. The average PL lifetime decreases as the temperature increases. The double-Boltzmann Fitting curve of the average PL lifetime discontinues at 130−150 K, as shown in Figure 4c, which is the same with the interruption of the integrated PL intensity. The excitation pulse width and repetition rate both have significant influence on photo-carrier lifetime in perovskite, which should be taken into consideration.[54] In our experiment, excitation laser pulse width is about 40 ps and the IRF is about 120 ps. Thus, there is only the exciton considered in the following photo-carriers thermally kinetic analysis, where the biexciton and trion decay is ignored. This is because the exciton decay is about 300 ps in the perovskite $CsPbBr_3$ nanocrystal, while the biexciton and trion undergo much faster decay than the exciton, which could not be measured, limited by the ability of instrument resolution.

Ideally, electrons transit from the ground state (GS) to the excitonic state (ES) after photo-excitation and rapidly return to GS with simultaneous PL emission, as shown in Figure 4d, the green solid line with arrow. It could be called direct recombination for excitons, which contributes to the fast decay of PL. This decay is about 300 ps, which agrees well with the short time (τ_1 = 0.294 ns) obtained, and it is weakly dependent on temperature.[55−58] There are not only direct recombination but also indirect recombination for excitons. There are always defect states,[34,59] surface states,[35,60] or dark states[37,61] existing in the colloidal all-inorganic perovskite $CsPbBr_3$ nanocrystal, which are named and referred as trap states (TS)[62−64] henceforth. The photo-excited electrons on the ES could also be trapped by these TS. In addition, the trapped electrons could be detrapped back to the ES under thermal activation,[65] which followed the recombination with holes on the GS, as shown in Figure 4d, the red solid lines with arrows. The holes have similar kinetics with electrons, the orange solid lines with arrows. The recombination process is called indirect recombination for excitons because of including more paths of trapping and detrapping. The holes have heavier mass than electrons, which could result in a slower decay item. Thus, decay of electrons and holes is corresponding to the intermediate time (τ_2 = 1.261 ns) and long time (τ_3 = 6.054 ns), respectively. Relaxation of both electrons and holes contribute to the slow decay of PL. The temperature-dependent slow decay of PL could be fitted by the double-Boltzmann function, as shown in Figure S5d, because of thermal kinetic electrons and holes following Boltzmann distribution.

At the beginning of increasing temperature, much TS exposure, photo-excited electrons, and holes are very easily trapped by these TS. Thus, there mainly occurs indirect recombination. As temperature increases, the thermal effect could increase the TS and reduce the detrapping effect. Hence, less photo-excited electrons and holes could be detrapped from TS, resulting in less indirect recombination and more direct recombination for excitons. At the temperature of 130−150 K, the direct recombination balance with indirect recombination, as shown in Figure S5e. On continuously increasing the temperature, there mainly occurs direct recombination at high temperature. These could explain both curves of the temperature-dependent PL intensity and average PL lifetime.

CONCLUSIONS

To summarize, we have synthesized colloidal all-inorganic lead halide perovskite $CsPbBr_3$ nanocrystals by a solution method. The steady-state PL intensity performs as a linear function of excitation power and the spectra invariant at room temperature. The temperature-dependent PL intensity follows the Arrhenius equation. Temperature-dependent TRPL shows that there are two distinct different time scales, fast decay and slow decay. The TRPL curves could be fitted by the tri-exponential function with a short time constant (τ_1 = 0.294 ns), an intermediate time constant (τ_2 = 1.261 ns), and a long time constant (τ_3 = 6.054 ns). The short time corresponds to the direct recombination for excitons, which contributes to the PL fast decay in colloidal all-inorganic lead halide perovskite $CsPbBr_3$ nanocrystals. The intermediate (long) time constant corresponds to the photo-excited electrons (holes) path along trapping-detrapping-recombination with holes (electrons), contributing to the PL slow decay. The thermal effect could increase the TS and reduce the detrapping effect, changing the occupied percentage of indirect and direct recombination for excitons. The exciton mainly undergoes indirect recombination at low temperature, balance at the temperature of 130−150 K, and direct recombination at high temperature. Our experimental results provide insights into the direct and indirect recombination mechanism for excitons in colloidal all-inorganic lead halide perovskite nanocrystals and help to unravel their potential for high-performance optoelectronic devices.

DOI: 10.1021/acs.jpcc.9b04532
J. Phys. Chem. C 2019, 123, 19844−19850

■ ASSOCIATED CONTENT

Supporting Information

The Supporting Information is available free of charge on the ACS Publications website at DOI: 10.1021/acs.jpcc.9b04532.

Synthesis and characterization; photos of synthesized perovskite samples; experiment system and temperature increase; system noise and PL stability; peak position and width (fwhm); temperature-dependent lifetime of samples; framework of a kinetic model for recombination of excitons, electrons, and holes; and TEM images and size distributions of perovskite nanocrystals (PDF)

■ AUTHOR INFORMATION

Corresponding Authors

*E-mail: chenr@sustech.edu.cn (R.C.).
*E-mail: zhangxh@sustech.edu.cn (X.Z.).

ORCID

Xiaoli Zhang: 0000-0003-1492-2068
Xiaowei Sun: 0000-0002-2840-1880
Xinhai Zhang: 0000-0003-2913-1744

Author Contributions

H.S. and X.Z. contributed equally to this work.

Notes

The authors declare no competing financial interest.

■ ACKNOWLEDGMENTS

The authors would like to acknowledge the support of Shenzhen Peacock Team Project under grant no. KQTD20150717103136556 and the National Natural Science Foundation of China under grant no. 61704072, Shenzhen Basic Research Fund under grand no. JCYJ20170817112012493.

■ REFERENCES

(1) Bush, K. A.; Palmstrom, A. F.; Yu, Z. J.; Boccard, M.; Cheacharoen, R.; Mailoa, J. P.; McMeekin, D. P.; Hoye, R. L. Z.; Bailie, C. D.; Leijtens, T.; et al. 23.6%-Efficient Monolithic Perovskite/Silicon Tandem Solar Cells with Improved Stability. *Nat. Energy* **2017**, *2*, 17009.

(2) Meng, F.; Liu, X.; Cai, X.; Gong, Z.; Li, B.; Xie, W.; Li, M.; Chen, D.; Yip, H.-L.; Su, S.-J. Incorporation of Rubidium Cations into Blue Perovskite Quantum Dot Light-Emitting Diodes Via Fabr-Modified Multi-Cation Hot-Injection Method. *Nanoscale* **2019**, *11*, 1295−1303.

(3) Hu, F.; Zhang, H.; Sun, C.; Yin, C.; Lv, B.; Zhang, C.; Yu, W. W.; Wang, X.; Zhang, Y.; Xiao, M. Superior Optical Properties of Perovskite Nanocrystals as Single Photon Emitters. *ACS Nano* **2015**, *9*, 12410−12416.

(4) Obraztsov, P. A.; Lyashenko, D.; Chizhov, P. A.; Konishi, K.; Nemoto, N.; Kuwata-Gonokami, M.; Welch, E.; Obraztsov, A. N.; Zakhidov, A. Ultrafast Zero-Bias Photocurrent and Terahertz Emission in Hybrid Perovskites. *Commun. Phys.* **2018**, *1*, 14.

(5) Guzelturk, B.; Belisle, R. A.; Smith, M. D.; Bruening, K.; Prasanna, R.; Yuan, Y.; Gopalan, V.; Tassone, C. J.; Karunadasa, H. I.; McGehee, M. D.; et al. Terahertz Emission from Hybrid Perovskites Driven by Ultrafast Charge Separation and Strong Electron-Phonon Coupling. *Adv. Mater.* **2018**, *30*, 1704737.

(6) Lindenberg, H.; Polavarapu, L.; Sichert, J. A.; Susha, A. S.; Urban, A. S.; Rogach, A. L. Colloidal Lead Halide Perovskite Nanocrystals: Synthesis, Optical Properties and Applications. *NPG Asia Mater.* **2016**, *8*, No. e328.

(7) Zhou, L.; Liao, J.-F.; Huang, Z.-G.; Wei, J.-H.; Wang, X.-D.; Li, W.-G.; Chen, H.-Y.; Kuang, D.-B.; Su, C.-Y. A Highly Red-Emissive Lead-Free Indium-Based Perovskite Single Crystal for Sensitive Water Detection. *Angew. Chem., Int. Ed.* **2019**, *58*, 5277−5281.

(8) Gong, X.; Voznyy, O.; Jain, A.; Liu, W.; Sabatini, R.; Piontkowski, Z.; Walters, G.; Bappi, G.; Nokhrin, S.; Bushuyev, O.; Yuan, M.; Comin, R.; McCamant, D.; Kelley, S. O.; Sargent, E. H. Electron-Phonon Interaction in Efficient Perovskite Blue Emitters. *Nat. Mater.* **2018**, *17*, 550−556.

(9) Shi, H.; Zhang, X.; Sun, X.; Zhang, X. Phonon Mode Transformation in Size-Evolved Solution-Processed Inorganic Lead Halide Perovskite. *Nanoscale* **2018**, *10*, 9892−9898.

(10) Yang, B.; Chen, J.; Hong, F.; Mao, X.; Zheng, K.; Yang, S.; Li, Y.; Pullerits, T.; Deng, W.; Han, K. Lead-Free, Air-Stable All-Inorganic Cesium Bismuth Halide Perovskite Nanocrystals. *Angew. Chem., Int. Ed. Engl.* **2017**, *56*, 12471−12475.

(11) Cha, J.-H.; Han, J. H.; Yin, W.; Park, C.; Park, Y.; Ahn, T. K.; Cho, J. H.; Jung, D.-Y. Photoresponse of $CsPbBr_3$ and Cs_4PbBr_6 Perovskite Single Crystals. *J. Phys. Chem. Lett.* **2017**, *8*, 565−570.

(12) Fu, M.; Tamarat, P.; Trebbia, J. B.; Bodnarchuk, M. I.; Kovalenko, M. V.; Even, J.; Lounis, B. Unraveling Exciton-Phonon Coupling in Individual $FaPbI_3$ Nanocrystals Emitting near-Infrared Single Photons. *Nat. Commun.* **2018**, *9*, 3318.

(13) Lao, X.; Yang, Z.; Su, Z.; Wang, Z.; Ye, H.; Wang, M.; Yao, X.; Xu, S. Luminescence and Thermal Behaviors of Free and Trapped Excitons in Cesium Lead Halide Perovskite Nanosheets. *Nanoscale* **2018**, *10*, 9949−9956.

(14) Rainò, G.; Nedelcu, G.; Protesescu, L.; Bodnarchuk, M. I.; Kovalenko, M. V.; Mahrt, R. F.; Stöferle, T. Single Cesium Lead Halide Perovskite Nanocrystals at Low Temperature: Fast Single-Photon Emission, Reduced Blinking, and Exciton Fine Structure. *ACS Nano* **2016**, *10*, 2485−2490.

(15) Seth, S.; Ahmed, T.; Samanta, A. Photoluminescence Flickering and Blinking of Single $CsPbBr_3$ Perovskite Nanocrystals: Revealing Explicit Carrier Recombination Dynamics. *J. Phys. Chem. Lett.* **2018**, *9*, 7007−7014.

(16) Makarov, N. S.; Guo, S.; Isaienko, O.; Liu, W.; Robel, I.; Klimov, V. I. Spectral and Dynamical Properties of Single Excitons, Biexcitons, and Trions in Cesium-Lead-Halide Perovskite Quantum Dots. *Nano Lett.* **2016**, *16*, 2349−2362.

(17) Li, Y.; Ding, T.; Luo, X.; Chen, Z.; Liu, X.; Lu, X.; Wu, K. Biexciton Auger Recombination in Mono-Dispersed, Quantum-Confined $CsPbBr_3$ Perovskite Nanocrystals Obeys Universal Volume-Scaling. *Nano Res.* **2018**, *12*, 619−623.

(18) Canneson, D.; Shornikova, E. V.; Yakovlev, D. R.; Rogge, T.; Mitioglu, A. A.; Ballottin, M. V.; Christianen, P. C. M.; Lhuillier, E.; Bayer, M.; Biadala, L. Negatively Charged and Dark Excitons in $CsPbBr_3$ Perovskite Nanocrystals Revealed by High Magnetic Fields. *Nano Lett.* **2017**, *17*, 6177−6183.

(19) Chen, L.; Li, B.; Zhang, C.; Huang, X.; Wang, X.; Xiao, M. Composition-Dependent Energy Splitting between Bright and Dark Excitons in Lead Halide Perovskite Nanocrystals. *Nano Lett.* **2018**, *18*, 2074−2080.

(20) Xu, K.; Vliem, J. F.; Meijerink, A. Long-Lived Dark Exciton Emission in Mn-Doped $CsPbCl_3$ Perovskite Nanocrystals. *J. Phys. Chem. C* **2018**, *123*, 979−984.

(21) Luo, J.; Wang, X.; Li, S.; Liu, J.; Guo, Y.; Niu, G.; Yao, L.; Fu, Y.; Gao, L.; Dong, Q.; et al. Efficient and Stable Emission of Warm-White Light from Lead-Free Halide Double Perovskites. *Nature* **2018**, *563*, 541−545.

(22) Smith, M. D.; Karunadasa, H. I. White-Light Emission from Layered Halide Perovskites. *Acc. Chem. Res.* **2018**, *51*, 619−627.

(23) Correa-Baena, J.-P.; Luo, Y.; Brenner, T. M.; Snaider, J.; Sun, S.; Li, X.; Jensen, M. A.; Hartono, N. T. P.; Nienhaus, L.; Wieghold, S.; Poindexter, J. R.; Wang, S.; Meng, Y. S.; Wang, T.; Lai, B.; Holt, M. V.; Cai, Z.; Bawendi, M. G.; Huang, L.; Buonassisi, T.; Fenning, D. P.; et al. Homogenized halides and alkali cation segregation in alloyed organic-inorganic perovskites. *Science* **2019**, *363*, 627−631.

(24) Chakrabartty, J.; Harnagea, C.; Celikin, M.; Rosei, F.; Nechache, R. Improved Photovoltaic Performance from Inorganic

DOI: 10.1021/acs.jpcc.9b04532
J. Phys. Chem. C 2019, 123, 19844−19850

Perovskite Oxide Thin Films with Mixed Crystal Phases. *Nat. Photonics* **2018**, *12*, 271−276.
(25) He, H.; Yu, Q.; Li, H.; Li, J.; Si, J.; Jin, Y.; Wang, N.; Wang, J.; He, J.; Wang, X.; et al. Exciton Localization in Solution-Processed Organolead Trihalide Perovskites. *Nat. Commun.* **2016**, *7*, 10896.
(26) Ye, H. G.; Su, Z. C.; Tang, F.; Chen, G. D.; Wang, J.; Xu, K.; Xu, S. J. Role of Free Electrons in Phosphorescence in N-Type Wide Bandgap Semiconductors. *Phys. Chem. Chem. Phys.* **2017**, *19*, 30332−30338.
(27) Aneesh, J.; Swarnkar, A.; Kumar Ravi, V.; Sharma, R.; Nag, A.; Adarsh, K. V. Ultrafast Exciton Dynamics in Colloidal $CsPbBr_3$ Perovskite Nanocrystals: Biexciton Effect and Auger Recombination. *J. Phys. Chem. C* **2017**, *121*, 4734−4739.
(28) Bacher, G.; Weigand, R.; Kulakovskii, V. D.; Gippius, N. A.; Forchel, A.; Leonardi, K.; Hommel, D. Biexciton Versus Exciton Lifetime in a Single Semiconductor Quantum Dot. *Phys. Rev. Lett.* **1999**, *83*, 4417.
(29) Kumawat, N. K.; Dey, A.; Kumar, A.; Gopinathan, S. P.; Narasimhan, K. L.; Kabra, D. Band Gap Tuning of $CH_3NH_3Pb(Br_{(1-X)}Cl_x)_3$ Hybrid Perovskite for Blue Electroluminescence. *ACS Appl. Mater. Interfaces* **2015**, *7*, 13119−13124.
(30) Mondal, N.; De, A.; Samanta, A. Biexciton Generation and Dissociation Dynamics in Formamidinium- and Chloride-Doped Cesium Lead Iodide Perovskite Nanocrystals. *J. Phys. Chem. Lett.* **2018**, *9*, 3673−3679.
(31) Nakahara, S.; Tahara, H.; Yumoto, G.; Kawawaki, T.; Saruyama, M.; Sato, R.; Teranishi, T.; Kanemitsu, Y. Suppression of Trion Formation in $CsPbBr_3$ Perovskite Nanocrystals by Postsynthetic Surface Modification. *J. Phys. Chem. C* **2018**, *122*, 22188−22193.
(32) Li, B.; Huang, H.; Zhang, G.; Yang, C.; Guo, W.; Chen, R.; Qin, C.; Gao, Y.; Biju, V. P.; Rogach, A. L.; et al. Excitons and Biexciton Dynamics in Single $CsPbBr_3$ Perovskite Quantum Dots. *J. Phys. Chem. Lett.* **2018**, *9*, 6934−6940.
(33) Wang, J.; Ding, T.; Leng, J.; Jin, S.; Wu, K. "Intact" Carrier Doping by Pump-Pump-Probe Spectroscopy in Combination with Interfacial Charge Transfer: A Case Study of $CsPbBr_3$ Nanocrystals. *J. Phys. Chem. Lett.* **2018**, *9*, 3372−3377.
(34) D'Innocenzo, V.; Srimath Kandada, A. R.; De Bastiani, M.; Gandini, M.; Petrozza, A. Tuning the Light Emission Properties by Band Gap Engineering in Hybrid Lead Halide Perovskite. *J. Am. Chem. Soc.* **2014**, *136*, 17730.
(35) Naghadeh, S. B.; Luo, B.; Pu, Y.-C.; Schwartz, Z.; Hollingsworth, W. R.; Lindley, S. A.; Brewer, A. S.; Ayzner, A. L.; Zhang, J. Z. Size Dependence of Charge Carrier Dynamics in Organometal Halide Perovskite Nanocrystals: Deciphering Radiative Versus Nonradiative Components. *J. Phys. Chem. C* **2019**, *123*, 4610−4619.
(36) Wang, Y.; Zhi, M.; Chang, Y.-Q.; Zhang, J.-P.; Chan, Y. Stable, Ultralow Threshold Amplified Spontaneous Emission from $CsPbBr_3$ Nanoparticles Exhibiting Trion Gain. *Nano Lett.* **2018**, *18*, 4976−4984.
(37) Chirvony, V. S.; González-Carrero, S.; Suárez, I.; Galian, R. E.; Sessolo, M.; Bolink, H. J.; Martínez-Pastor, J. P.; Pérez-Prieto, J. Delayed Luminescence in Lead Halide Perovskite Nanocrystals. *J. Phys. Chem. C* **2017**, *121*, 13381−13390.
(38) Dey, A.; Rathod, P.; Kabra, D. Role of Localized States in Photoluminescence Dynamics of High Optical Gain $CsPbBr_3$ Nanocrystals. *Adv. Opt. Mater.* **2018**, *6*, 1800109.
(39) Sharma, D. K.; Hirata, S.; Biju, V.; Vacha, M. Stark Effect and Environment-Induced Modulation of Emission in Single Halide Perovskite Nanocrystals. *ACS Nano* **2019**, *13*, 624−632.
(40) Singh, S.; Li, C.; Panzer, F.; Narasimhan, K. L.; Graeser, A.; Gujar, T. P.; Köhler, A.; Thelakkat, M.; Huettner, S.; Kabra, D. Effect of Thermal and Structural Disorder on the Electronic Structure of Hybrid Perovskite Semiconductor $CH_3NH_3PbI_3$. *J. Phys. Chem. Lett.* **2016**, *7*, 3014−3021.
(41) Jones, M.; Lo, S. S.; Scholes, G. D. Signatures of Exciton Dynamics and Carrier Trapping in the Time-Resolved Photoluminescence of Colloidal CdSe Nanocrystals. *J. Phys. Chem. C* **2009**, *113*, 18632−18642.
(42) He, Y.-M.; Iff, O.; Lundt, N.; Baumann, V.; Davanco, M.; Srinivasan, K.; Hofling, S.; Schneider, C. Cascaded Emission of Single Photons from the Biexciton in Monolayered WSe_2. *Nat. Commun.* **2016**, *7*, 13409.
(43) Marchioro, A.; Whitham, P. J.; Knowles, K. E.; Kilburn, T. B.; Reid, P. J.; Gamelin, D. R. Tunneling in the Delayed Luminescence of Colloidal CdSe, Cu^+-Doped CdSe, and $CuInS_2$ Semiconductor Nanocrystals and Relationship to Blinking. *J. Phys. Chem. C* **2016**, *120*, 27040−27049.
(44) Aldakov, D.; Reiss, P. Safer-by-Design Fluorescent Nanocrystals: Metal Halide Perovskites Vs Semiconductor Quantum Dots. *J. Phys. Chem. C* **2019**, *123*, 12527−12541.
(45) Bimberg, D.; Sondergeld, M.; Grobe, E. Thermal Dissociation of Excitons Bounds to Neutral Acceptors in High-Purity Gaas. *Phys. Rev. B* **1971**, *4*, 3451−3455.
(46) Gibson, N. A.; Koscher, B. A.; Alivisatos, A. P.; Leone, S. R. Excitation Intensity Dependence of Photoluminescence Blinking in $CsPbBr_3$ Perovskite Nanocrystals. *J. Phys. Chem. C* **2018**, *122*, 12106−12113.
(47) Wang, Y.; Zhi, M.; Chan, Y. Delayed Exciton Formation Involving Energetically Shallow Trap States in Colloidal $CsPbBr_3$ Quantum Dots. *J. Phys. Chem. C* **2017**, *121*, 28498−28505.
(48) Kim, J. C.; Wake, D. R.; Wolfe, J. P. Thermodynamics of Biexcitons in a Gaas Quantum Well. *Phys. Rev. B* **1994**, *50*, 15099−15107.
(49) Bakthavatsalam, R.; Biswas, A.; Chakali, M.; Bangal, P. R.; Kore, B. P.; Kundu, J. Temperature-Dependent Photoluminescence and Energy-Transfer Dynamics in Mn^{2+}-Doped $(C_4H_9NH_3)_2PbBr_4$ Two-Dimensional (2D) Layered Perovskite. *J. Phys. Chem. C* **2019**, *123*, 4739−4748.
(50) Tsai, H.; Asadpour, R.; Blancon, J.-C.; Stoumpos, C. C.; Durand, O.; Strzalka, J. W.; Chen, B.; Verduzco, R.; Ajayan, P. M.; Tretiak, S.; Even, J.; Alam, M. A.; Kanatzidis, M. G.; Nie, W.; Mohite, A. D. Light-Induced Lattice Expansion Leads to High-Efficiency Perovskite Solar Cells. *Science* **2018**, *360*, 67−70.
(51) Shen, W.; Ruan, L.; Shen, Z.; Deng, Z. Reversible Light-Mediated Compositional and Structural Transitions between $CsPbBr_3$ and $CsPb_2Br_5$ Nanosheets. *Chem. Commun.* **2018**, *54*, 2804−2807.
(52) Davies, C. L.; Filip, M. R.; Patel, J. B.; Crothers, T. W.; Verdi, C.; Wright, A. D.; Milot, R. L.; Giustino, F.; Johnston, M. B.; Herz, L. M. Bimolecular Recombination in Methylammonium Lead Triiodide Perovskite Is an Inverse Absorption Process. *Nat. Commun.* **2018**, *9*, 293.
(53) Segall, B.; Mahan, G. D. Phonon-Assisted Recombination of Free Excitons in Compound Semiconductors. *Phys. Rev.* **1968**, *171*, 935−948.
(54) Kudriashova, L. G.; Kiermasch, D.; Rieder, P.; Campbell, M.; Tvingstedt, K.; Baumann, A.; Astakhov, G. V.; Dyakonov, V. Impact of Interfaces and Laser Repetition Rate on Photocarrier Dynamics in Lead Halide Perovskites. *J. Phys. Chem. Lett.* **2017**, *8*, 4698−4703.
(55) Chirvony, V. S.; Martínez-Pastor, J. P. Trap-Limited Dynamics of Excited Carriers and Interpretation of the Photoluminescence Decay Kinetics in Metal Halide Perovskites. *J. Phys. Chem. Lett.* **2018**, *9*, 4955−4962.
(56) Rabouw, F. T.; van der Bok, J. C.; Spinicelli, P.; Mahler, B.; Nasilowski, M.; Pedetti, S.; Dubertret, B.; Vanmaekelbergh, D. Temporary Charge Carrier Separation Dominates the Photoluminescence Decay Dynamics of Colloidal CdSe Nanoplatelets. *Nano Lett.* **2016**, *16*, 2047−2053.
(57) Stranks, S. D.; Burlakov, V. M.; Leijtens, T.; Ball, J. M.; Goriely, A.; Snaith, H. J. Recombination Kinetics in Organic-Inorganic Perovskites: Excitons, Free Charge, and Subgap States. *Phys. Rev. Appl.* **2014**, *2*, 034007.
(58) Whitham, P. J.; Marchioro, A.; Knowles, K. E.; Kilburn, T. B.; Reid, P. J.; Gamelin, D. R. Single-Particle Photoluminescence Spectra, Blinking, and Delayed Luminescence of Colloidal $CuInS_2$ Nanocrystals. *J. Phys. Chem. C* **2016**, *120*, 17136−17142.

DOI: 10.1021/acs.jpcc.9b04532
J. Phys. Chem. C 2019, 123, 19844−19850

(59) Dänekamp, B.; Droseros, N.; Palazon, F.; Sessolo, M.; Banerji, N.; Bolink, H. J. Efficient Photo- and Electroluminescence by Trap States Passivation in Vacuum-Deposited Hybrid Perovskite Thin Films. *ACS Appl. Mater. Interfaces* **2018**, *10*, 36187−36193.
(60) Koscher, B. A.; Swabeck, J. K.; Bronstein, N. D.; Alivisatos, A. P. Essentially Trap-Free $CsPbBr_3$ Colloidal Nanocrystals by Postsynthetic Thiocyanate Surface Treatment. *J. Am. Chem. Soc.* **2017**, *139*, 6566−6569.
(61) Becker, M. A.; Scarpelli, L.; Nedelcu, G.; Rainò, G.; Masia, F.; Borri, P.; Stöferle, T.; Kovalenko, M. V.; Langbein, W.; Mahrt, R. F. Long Exciton Dephasing Time and Coherent Phonon Coupling in $CsPbBr_2Cl$ Perovskite Nanocrystals. *Nano Lett.* **2018**, *18*, 7546−7551.
(62) Yao, J.-S.; Ge, J.; Han, B.-N.; Wang, K.-H.; Yao, H.-B.; Yu, H.-L.; Li, J.-H.; Zhu, B.-S.; Song, J.-Z.; Chen, C.; et al. Ce^{3+}-Doping to Modulate Photoluminescence Kinetics for Efficient $CsPbBr_3$ Nanocrystals Based Light-Emitting Diodes. *J. Am. Chem. Soc.* **2018**, *140*, 3626−3634.
(63) Yamada, Y.; Yamada, T.; Shimazaki, A.; Wakamiya, A.; Kanemitsu, Y. Interfacial Charge-Carrier Trapping in $CH_3NH_3PbI_3$-Based Heterolayered Structures Revealed by Time-Resolved Photoluminescence Spectroscopy. *J. Phys. Chem. Lett.* **2016**, *7*, 1972−1977.
(64) Marchioro, A.; Whitham, P. J.; Nelson, H. D.; De Siena, M. C.; Knowles, K. E.; Polinger, V. Z.; Reid, P. J.; Gamelin, D. R. Strong Dependence of Quantum-Dot Delayed Luminescence on Excitation Pulse Width. *J. Phys. Chem. Lett.* **2017**, *8*, 3997−4003.
(65) Yuan, X.; Ji, S.; De Siena, M. C.; Fei, L.; Zhao, Z.; Wang, Y.; Li, H.; Zhao, J.; Gamelin, D. R. Photoluminescence Temperature Dependence, Dynamics, and Quantum Efficiencies in Mn^{2+}-Doped $CsPbCl_3$ Perovskite Nanocrystals with Varied Dopant Concentration. *Chem. Mater.* **2017**, *29*, 8003−8011.

DOI: 10.1021/acs.jpcc.9b04532
J. Phys. Chem. C 2019, 123, 19844−19850